Measurements of the Angular Distributions of Muons from Υ Decays in $p\bar{p}$ Collisions at $\sqrt{s} = 1.96$ TeV

T. Aaltonen,[21] B. Álvarez González,[9,aa] S. Amerio,[40a] D. Amidei,[32] A. Anastassov,[15,y] A. Annovi,[17] J. Antos,[12] G. Apollinari,[15] J. A. Appel,[15] T. Arisawa,[54] A. Artikov,[13] J. Asaadi,[49] W. Ashmanskas,[15] B. Auerbach,[57] A. Aurisano,[49] F. Azfar,[39] W. Badgett,[15] T. Bae,[25] A. Barbaro-Galtieri,[26] V. E. Barnes,[44] B. A. Barnett,[23] P. Barria,[42c,42a] P. Bartos,[12] M. Bauce,[40b,40a] F. Bedeschi,[42a] S. Behari,[23] G. Bellettini,[42b,42a] J. Bellinger,[56] D. Benjamin,[14] A. Beretvas,[15] A. Bhatti,[46] D. Bisello,[40b,40a] I. Bizjak,[28] K. R. Bland,[5] B. Blumenfeld,[23] A. Bocci,[14] A. Bodek,[45] D. Bortoletto,[44] J. Boudreau,[43] A. Boveia,[11] L. Brigliadori,[6b,6a] C. Bromberg,[33] E. Brucken,[21] J. Budagov,[13] H. S. Budd,[45] K. Burkett,[15] G. Busetto,[40b,40a] P. Bussey,[19] A. Buzatu,[31] A. Calamba,[10] C. Calancha,[29] S. Camarda,[4] M. Campanelli,[28] M. Campbell,[32] F. Canelli,[11,15] B. Carls,[22] D. Carlsmith,[56] R. Carosi,[42a] S. Carrillo,[16,n] S. Carron,[15] B. Casal,[9,l] M. Casarsa,[50a] A. Castro,[6b,6a] P. Catastini,[20] D. Cauz,[50a] V. Cavaliere,[22] M. Cavalli-Sforza,[4] A. Cerri,[26,g] L. Cerrito,[28,t] Y. C. Chen,[1] M. Chertok,[7] G. Chiarelli,[42a] G. Chlachidze,[15] F. Chlebana,[15] K. Cho,[25] D. Chokheli,[13] W. H. Chung,[56] Y. S. Chung,[45] M. A. Ciocci,[42c,42a] A. Clark,[18] C. Clarke,[55] G. Compostella,[40b,40a] M. E. Convery,[15] J. Conway,[7] M. Corbo,[15] M. Cordelli,[17] C. A. Cox,[7] D. J. Cox,[7] F. Crescioli,[42b,42a] J. Cuevas,[9,aa] R. Culbertson,[15] D. Dagenhart,[15] N. d'Ascenzo,[15,x] M. Datta,[15] P. de Barbaro,[45] M. Dell'Orso,[42b,42a] L. Demortier,[46] M. Deninno,[6a] F. Devoto,[21] M. d'Errico,[40b,40a] A. Di Canto,[42a] B. Di Ruzza,[15] J. R. Dittmann,[5] M. D'Onofrio,[27] S. Donati,[42b,42a] P. Dong,[15] M. Dorigo,[50a] T. Dorigo,[40a] K. Ebina,[54] A. Elagin,[49] A. Eppig,[32] R. Erbacher,[7] S. Errede,[22] N. Ershaidat,[15,ee] R. Eusebi,[49] S. Farrington,[39] M. Feindt,[24] J. P. Fernandez,[29] R. Field,[16] G. Flanagan,[15,v] R. Forrest,[7] M. J. Frank,[5] M. Franklin,[20] J. C. Freeman,[15] Y. Funakoshi,[54] I. Furic,[16] M. Gallinaro,[46] J. E. Garcia,[18] A. F. Garfinkel,[44] P. Garosi,[42c,42a] H. Gerberich,[22] E. Gerchtein,[15] S. Giagu,[47a] V. Giakoumopoulou,[3] P. Giannetti,[42a] K. Gibson,[43] C. M. Ginsburg,[15] N. Giokaris,[3] P. Giromini,[17] G. Giurgiu,[23] V. Glagolev,[13] D. Glenzinski,[15] M. Gold,[35] D. Goldin,[49] N. Goldschmidt,[16] A. Golossanov,[15] G. Gomez,[9] G. Gomez-Ceballos,[30] M. Goncharov,[30] O. González,[29] I. Gorelov,[35] A. T. Goshaw,[14] K. Goulianos,[46] S. Grinstein,[4] C. Grosso-Pilcher,[11] R. C. Group,[53,15] J. Guimaraes da Costa,[20] S. R. Hahn,[15] E. Halkiadakis,[48] A. Hamaguchi,[38] J. Y. Han,[45] F. Happacher,[17] K. Hara,[51] D. Hare,[48] M. Hare,[52] R. F. Harr,[55] K. Hatakeyama,[5] C. Hays,[39] M. Heck,[24] J. Heinrich,[41] M. Herndon,[56] S. Hewamanage,[5] A. Hocker,[15] W. Hopkins,[15,h] D. Horn,[24] S. Hou,[1] R. E. Hughes,[a36] M. Hurwitz,[11] U. Husemann,[57] N. Hussain,[31] M. Hussein,[33] J. Huston,[33] G. Introzzi,[42a] M. Iori,[47b,47a] A. Ivanov,[7,q] E. James,[15] D. Jang,[10] B. Jayatilaka,[14] E. J. Jeon,[25] S. Jindariani,[15] M. Jones,[44] K. K. Joo,[25] S. Y. Jun,[10] T. R. Junk,[15] T. Kamon,[25,49] P. E. Karchin,[55] A. Kasmi,[5] Y. Kato,[38,p] W. Ketchum,[11] J. Keung,[41] V. Khotilovich,[49] B. Kilminster,[15] D. H. Kim,[25] H. S. Kim,[25] J. E. Kim,[25] M. J. Kim,[17] S. B. Kim,[25] S. H. Kim,[51] Y. K. Kim,[11] Y. J. Kim,[25] N. Kimura,[54] M. Kirby,[15] S. Klimenko,[16] K. Knoepfel,[15] K. Kondo,[54,a] D. J. Kong,[25] J. Konigsberg,[16] A. V. Kotwal,[14] M. Kreps,[24] J. Kroll,[41] D. Krop,[11] M. Kruse,[14] V. Krutelyov,[49,d] T. Kuhr,[24] M. Kurata,[51] S. Kwang,[11] A. T. Laasanen,[44] S. Lami,[42a] S. Lammel,[15] M. Lancaster,[28] R. L. Lander,[7] K. Lannon,[a36,z] A. Lath,[48] G. Latino,[42c,42a] T. LeCompte,[2] E. Lee,[49] H. S. Lee,[11,r] J. S. Lee,[25] S. W. Lee,[49,cc] S. Leo,[42b,42a] S. Leone,[42a] J. D. Lewis,[15] A. Limosani,[14,u] C.-J. Lin,[26] M. Lindgren,[15] E. Lipeles,[41] A. Lister,[18] D. O. Litvintsev,[15] C. Liu,[43] H. Liu,[53] Q. Liu,[44] T. Liu,[15] S. Lockwitz,[57] A. Loginov,[57] D. Lucchesi,[40b,40a] J. Lueck,[24] P. Lujan,[26] P. Lukens,[15] G. Lungu,[46] J. Lys,[26] R. Lysak,[12,f] R. Madrak,[15] K. Maeshima,[15] P. Maestro,[42c,42a] S. Malik,[46] G. Manca,[27,b] A. Manousakis-Katsikakis,[3] F. Margaroli,[47a] C. Marino,[24] M. Martínez,[4] P. Mastrandrea,[47a] K. Matera,[22] M. E. Mattson,[55] A. Mazzacane,[15] P. Mazzanti,[6a] K. S. McFarland,[45] P. McIntyre,[49] R. McNulty,[27,k] A. Mehta,[27] P. Mehtala,[21] C. Mesropian,[46] T. Miao,[15] D. Mietlicki,[32] A. Mitra,[1] H. Miyake,[51] S. Moed,[15] N. Moggi,[6a] M. N. Mondragon,[15,n] C. S. Moon,[25] R. Moore,[15] M. J. Morello,[42d,42a] J. Morlock,[24] P. Movilla Fernandez,[15] A. Mukherjee,[15] Th. Muller,[24] P. Murat,[15] M. Mussini,[6b,6a] J. Nachtman,[15,o] Y. Nagai,[51] J. Naganoma,[54] I. Nakano,[37] A. Napier,[52] J. Nett,[49] C. Neu,[53] M. S. Neubauer,[22] J. Nielsen,[26,e] L. Nodulman,[2] S. Y. Noh,[25] O. Norniella,[22] L. Oakes,[39] S. H. Oh,[14] Y. D. Oh,[25] I. Oksuzian,[53] T. Okusawa,[38] R. Orava,[21] L. Ortolan,[4] S. Pagan Griso,[40b,40a] C. Pagliarone,[50a] E. Palencia,[9,g] V. Papadimitriou,[15] A. A. Paramonov,[2] J. Patrick,[15] G. Pauletta,[50b,50a] M. Paulini,[10] C. Paus,[30] D. E. Pellett,[7] A. Penzo,[50a] T. J. Phillips,[14] G. Piacentino,[42a] E. Pianori,[41] J. Pilot,[a36] K. Pitts,[22] C. Plager,[8] L. Pondrom,[56] S. Poprocki,[15,h] K. Potamianos,[44] F. Prokoshin,[13,dd] A. Pranko,[26] F. Ptohos,[17,i] G. Punzi,[42b,42a] A. Rahaman,[43] V. Ramakrishnan,[56] N. Ranjan,[44] I. Redondo,[29] P. Renton,[39] M. Rescigno,[47a] T. Riddick,[28] F. Rimondi,[6b,6a] L. Ristori,[42a,15] A. Robson,[19] T. Rodrigo,[9] T. Rodriguez,[41] E. Rogers,[22] S. Rolli,[52,j] R. Roser,[15] F. Ruffini,[42c,42a] A. Ruiz,[9] J. Russ,[10] V. Rusu,[15] A. Safonov,[49] W. K. Sakumoto,[45] Y. Sakurai,[54] L. Santi,[50b,50a] K. Sato,[51] V. Saveliev,[15,x] A. Savoy-Navarro,[15,bb] P. Schlabach,[15] A. Schmidt,[24] E. E. Schmidt,[15] T. Schwarz,[15]

L. Scodellaro,[9] A. Scribano,[42c,42a] F. Scuri,[42a] S. Seidel,[35] Y. Seiya,[38] A. Semenov,[13] F. Sforza,[42c,42a] S. Z. Shalhout,[7] T. Shears,[27] P. F. Shepard,[43] M. Shimojima,[51,w] M. Shochet,[11] I. Shreyber-Tecker,[34] A. Simonenko,[13] P. Sinervo,[31] K. Sliwa,[52] J. R. Smith,[7] F. D. Snider,[15] A. Soha,[15] V. Sorin,[4] H. Song,[43] P. Squillacioti,[42c,42a] M. Stancari,[15] R. St. Denis,[19] B. Stelzer,[31] O. Stelzer-Chilton,[31] D. Stentz,[15,y] J. Strologas,[35] G. L. Strycker,[32] Y. Sudo,[51] A. Sukhanov,[15] I. Suslov,[13] K. Takemasa,[51] Y. Takeuchi,[51] J. Tang,[11] M. Tecchio,[32] P. K. Teng,[1] J. Thom,[15,h] J. Thome,[10] G. A. Thompson,[22] E. Thomson,[41] D. Toback,[49] S. Tokar,[12] K. Tollefson,[33] T. Tomura,[51] D. Tonelli,[15] S. Torre,[17] D. Torretta,[15] P. Totaro,[40a] M. Trovato,[42d,42a] F. Ukegawa,[51] S. Uozumi,[25] A. Varganov,[32] F. Vázquez,[16,o] G. Velev,[15] C. Vellidis,[15] M. Vidal,[44] I. Vila,[9] R. Vilar,[9] J. Vizán,[9] M. Vogel,[35] G. Volpi,[17] P. Wagner,[41] R. L. Wagner,[15] T. Wakisaka,[38] R. Wallny,[8] S. M. Wang,[1] A. Warburton,[31] D. Waters,[28] W. C. Wester III,[15] D. Whiteson,[41,c] A. B. Wicklund,[2] E. Wicklund,[15] S. Wilbur,[11] F. Wick,[24] H. H. Williams,[41] J. S. Wilson,[a36] P. Wilson,[15] B. L. Winer,[a36] P. Wittich,[15,h] S. Wolbers,[15] H. Wolfe,[a36] T. Wright,[32] X. Wu,[18] Z. Wu,[5] K. Yamamoto,[38] D. Yamato,[38] T. Yang,[15] U. K. Yang,[11,s] Y. C. Yang,[25] W.-M. Yao,[26] G. P. Yeh,[15] K. Yi,[15,o] J. Yoh,[15] K. Yorita,[54] T. Yoshida,[38,m] G. B. Yu,[14] I. Yu,[25] S. S. Yu,[15] J. C. Yun,[15] A. Zanetti,[50a] Y. Zeng,[14] C. Zhou,[14] and S. Zucchelli[6b,6a]

(CDF Collaboration)

[1]*Institute of Physics, Academia Sinica, Taipei, Taiwan 11529, Republic of China*
[2]*Argonne National Laboratory, Argonne, Illinois 60439, USA*
[3]*University of Athens, 157 71 Athens, Greece*
[4]*Institut de Fisica d'Altes Energies, ICREA, Universitat Autonoma de Barcelona, E-08193, Bellaterra (Barcelona), Spain*
[5]*Baylor University, Waco, Texas 76798, USA*
[6a]*Istituto Nazionale di Fisica Nucleare Bologna, I-40127 Bologna, Italy*
[6b]*University of Bologna, I-40127 Bologna, Italy*
[7]*University of California, Davis, Davis, California 95616, USA*
[8]*University of California, Los Angeles, Los Angeles, California 90024, USA*
[9]*Instituto de Fisica de Cantabria, CSIC-University of Cantabria, 39005 Santander, Spain*
[10]*Carnegie Mellon University, Pittsburgh, Pennsylvania 15213, USA*
[11]*Enrico Fermi Institute, University of Chicago, Chicago, Illinois 60637, USA*
[12]*Comenius University, 842 48 Bratislava, Slovakia; Institute of Experimental Physics, 040 01 Kosice, Slovakia*
[13]*Joint Institute for Nuclear Research, RU-141980 Dubna, Russia*
[14]*Duke University, Durham, North Carolina 27708, USA*
[15]*Fermi National Accelerator Laboratory, Batavia, Illinois 60510, USA*
[16]*University of Florida, Gainesville, Florida 32611, USA*
[17]*Laboratori Nazionali di Frascati, Istituto Nazionale di Fisica Nucleare, I-00044 Frascati, Italy*
[18]*University of Geneva, CH-1211 Geneva 4, Switzerland*
[19]*Glasgow University, Glasgow G12 8QQ, United Kingdom*
[20]*Harvard University, Cambridge, Massachusetts 02138, USA*
[21]*Division of High Energy Physics, Department of Physics, University of Helsinki and Helsinki Institute of Physics, FIN-00014, Helsinki, Finland*
[22]*University of Illinois, Urbana, Illinois 61801, USA*
[23]*The Johns Hopkins University, Baltimore, Maryland 21218, USA*
[24]*Institut für Experimentelle Kernphysik, Karlsruhe Institute of Technology, D-76131 Karlsruhe, Germany*
[25]*Center for High Energy Physics: Kyungpook National University, Daegu 702-701, Korea; Seoul National University, Seoul 151-742, Korea; Sungkyunkwan University, Suwon 440-746, Korea; Korea Institute of Science and Technology Information, Daejeon 305-806, Korea; Chonnam National University, Gwangju 500-757, Korea; Chonbuk National University, Jeonju 561-756, Korea*
[26]*Ernest Orlando Lawrence Berkeley National Laboratory, Berkeley, California 94720, USA*
[27]*University of Liverpool, Liverpool L69 7ZE, United Kingdom*
[28]*University College London, London WC1E 6BT, United Kingdom*
[29]*Centro de Investigaciones Energeticas Medioambientales y Tecnologicas, E-28040 Madrid, Spain*
[30]*Massachusetts Institute of Technology, Cambridge, Massachusetts 02139, USA*
[31]*Institute of Particle Physics: McGill University, Montréal, Québec, Canada H3A 2T8; Simon Fraser University, Burnaby, British Columbia, Canada V5A 1S6; University of Toronto, Toronto, Ontario, Canada M5S 1A7; and TRIUMF, Vancouver, British Columbia, Canada V6T 2A3*
[32]*University of Michigan, Ann Arbor, Michigan 48109, USA*
[33]*Michigan State University, East Lansing, Michigan 48824, USA*
[34]*Institution for Theoretical and Experimental Physics, ITEP, Moscow 117259, Russia*
[35]*University of New Mexico, Albuquerque, New Mexico 87131, USA*
[a36]*The Ohio State University, Columbus, Ohio 43210, USA*

[37]Okayama University, Okayama 700-8530, Japan
[38]Osaka City University, Osaka 588, Japan
[39]University of Oxford, Oxford OX1 3RH, United Kingdom
[40a]Istituto Nazionale di Fisica Nucleare, Sezione di Padova-Trento, I-35131 Padova, Italy
[40b]University of Padova, I-35131 Padova, Italy
[41]University of Pennsylvania, Philadelphia, Pennsylvania 19104, USA
[42a]Istituto Nazionale di Fisica Nucleare Pisa, I-56127 Pisa, Italy
[42b]University of Pisa, I-56127 Pisa, Italy
[42c]University of Siena, I-56127 Pisa, Italy
[42d]Scuola Normale Superiore, I-56127 Pisa, Italy
[43]University of Pittsburgh, Pittsburgh, Pennsylvania 15260, USA
[44]Purdue University, West Lafayette, Indiana 47907, USA
[45]University of Rochester, Rochester, New York 14627, USA
[46]The Rockefeller University, New York, New York 10065, USA
[47a]Istituto Nazionale di Fisica Nucleare, Sezione di Roma 1, I-00185 Roma, Italy
[47b]Sapienza Università di Roma, I-00185 Roma, Italy
[48]Rutgers University, Piscataway, New Jersey 08855, USA
[49]Texas A&M University, College Station, Texas 77843, USA
[50a]Istituto Nazionale di Fisica Nucleare Trieste/Udine, I-34100 Trieste, I-33100 Udine, Italy
[50b]University of Udine, I-33100 Udine, Italy
[51]University of Tsukuba, Tsukuba, Ibaraki 305, Japan
[52]Tufts University, Medford, Massachusetts 02155, USA
[53]University of Virginia, Charlottesville, Virginia 22906, USA
[54]Waseda University, Tokyo 169, Japan
[55]Wayne State University, Detroit, Michigan 48201, USA
[56]University of Wisconsin, Madison, Wisconsin 53706, USA
[57]Yale University, New Haven, Connecticut 06520, USA
(Received 6 December 2011; published 11 April 2012)

The angular distributions of muons from $\Upsilon(1S, 2S, 3S) \to \mu^+\mu^-$ decays are measured using data from $p\bar{p}$ collisions at $\sqrt{s} = 1.96$ TeV corresponding to an integrated luminosity of 6.7 fb^{-1} and collected with the CDF II detector at the Fermilab Tevatron. This analysis is the first to report the full angular distributions as functions of transverse momentum p_T for Υ mesons in both the Collins-Soper and s-channel helicity frames. This is also the first measurement of the spin alignment of $\Upsilon(3S)$ mesons. Within the kinematic range of Υ rapidity $|y| < 0.6$ and p_T up to 40 GeV/c, the angular distributions are found to be nearly isotropic.

DOI: 10.1103/PhysRevLett.108.151802 PACS numbers: 13.20.Gd, 13.85.Ni, 14.40.Pq

Heavy quarkonium production in hadron collisions provides critical tests of quantum chromodynamics (QCD) because it involves both short-distance and long-distance contributions. The cross sections for direct charmonium and Υ production measured at the Tevatron in $p\bar{p}$ collisions [1] greatly exceeded the predictions from leading-order ''color singlet'' models [2]. Further measurements of spin alignment in J/ψ, ψ' [3] and Υ production [4] proved to be in dramatic disagreement with predictions of ''color octet'' models that were developed to explain the cross section results [5]. While spin alignment can provide very sensitive tests for QCD models, the measured elements of the spin-density matrix for the spin-1 Υ states depend critically on the choice of coordinate frame.

Recently, it has been pointed out that improved experimental measurements are needed to clarify this situation [6]. In general, the angular distribution of the μ^+ in the rest frame of an $\Upsilon \to \mu^+\mu^-$ decay can be written as [7]

$$\frac{dN}{d\Omega} \sim 1 + \lambda_\theta \cos^2\theta + \lambda_\varphi \sin^2\theta \cos 2\varphi + \lambda_{\theta\varphi} \sin 2\theta \cos\varphi, \quad (1)$$

in which θ is the polar angle measured with respect to a quantization axis, and φ is the azimuthal angle measured with respect to the production plane containing the Υ and the beam axis. The coefficients are directly related to the elements of the spin-density matrix for the ensemble of Υ states observed [8]. Previous studies at hadron colliders have measured only λ_θ in the s-channel helicity frame, where the quantization axis coincides with the direction of the Υ momentum and cannot be transformed into different coordinate frames without additional information. This precludes model-independent comparisons of results obtained in different coordinate frames or experimental environments. Improving on this experimental situation requires not only measuring all three coefficients, but also carrying out these measurements in multiple

coordinate frames. This would allow a comparison of quantities such as $\tilde{\lambda} = (\lambda_\theta + 3\lambda_\varphi)/(1 - \lambda_\varphi)$, which should have the same value in different coordinate frames [9]. Such a test would provide an important demonstration that observations have not been seriously biased due to poor determination of experimental acceptance or subtraction of highly nonisotropic backgrounds.

In this Letter, we report on the first analysis of angular distributions of muons from $\Upsilon(1S, 2S, 3S) \to \mu^+\mu^-$ decays produced in $p\bar{p}$ collisions carried out using this formalism: the distributions are quantified in both the s-channel helicity frame and in the Collins-Soper frame, which approximates, on average, the direction of the velocity of the colliding beams. It is also the first analysis to provide information on the angular distributions of muons in decays of the $\Upsilon(3S)$ state, which is more likely to be produced directly, rather than as a decay product of higher mass quarkonium states.

The $\Upsilon \to \mu^+\mu^-$ decays were collected using the CDF II detector, which reconstructs charged-particle tracks and measures their momenta using a six-layer silicon strip detector [10] and a large-volume drift chamber [11], both with approximate cylindrical geometry and positioned in a 1.4 T solenoidal magnetic field. The tracking detectors are surrounded by calorimeters and three separate muon detector subsystems. The central muon (CMU) system [12] consists of four layers of drift tubes that are located outside the hadron calorimeter and cover the central range of pseudorapidity $|\eta| < 0.6$. The central muon upgrade (CMP) system [13] comprises more layers of drift tubes and scintillators placed behind additional steel absorber material and covers approximately $|\eta| < 0.4$. Extended muon coverage in the forward region $0.6 < |\eta| < 1$ is provided by the central muon extension (CMX) subdetector which is also constructed from scintillators and drift tubes.

A three-level online event selection system (trigger) is used to identify events that contain oppositely charged dimuon candidates. The level-1 trigger requires two tracks with $p_T > 1.5$ GeV/c to be identified in the tracking chamber and to be geometrically correlated with activity in the CMU or CMX muon systems [14]. The level-2 trigger requires the muons to have opposite charge, and it requires that one of the muons have $p_T > 3$ GeV/c and that it be detected in both the CMU and CMP systems. Events satisfying the level-2 trigger are passed to the level-3 trigger system, which employs a version of the full event reconstruction software optimized for speed. The event selection used in the level-3 trigger requires the presence of two oppositely charged muon candidates with invariant mass in the range $8 < m(\mu^+\mu^-) < 12$ GeV/c^2. It requires one to be reconstructed in both CMU and CMP systems with $p_T > 4$ GeV/c and the other to be reconstructed in either the CMU or CMX detectors with $p_T > 3$ GeV/c. In this Letter, we refer to the trigger scenario that selects two central muons as "central-central," and the scenario that selects one central and one forward muon as "central-forward." From 6.7 fb^{-1} of integrated luminosity, the combination of these triggers provides an event sample containing approximately 550 000 $\Upsilon(1S)$, 150 000 $\Upsilon(2S)$, and 76 000 $\Upsilon(3S)$ decays.

The criteria used to select dimuon candidates closely follow those previously used in Ref. [15]. Muon candidates are reconstructed from tracks in the drift chamber that extrapolate to a track segment reconstructed in at least one of the muon detector systems. Geometric restrictions are imposed on muon candidates to ensure that they are contained in regions of the detector with well-measured trigger and track reconstruction efficiencies. Efficiencies for the level-1 trigger and for these selection criteria are measured using the unbiased track in $J/\psi \to \mu^+\mu^-$ decays that were recorded using a single-muon trigger. This analysis also makes use of information from the CMP muon system in the level-2 trigger. The efficiency for selecting such muons is measured using samples of $J/\psi \to \mu^+\mu^-$ decays obtained using triggers that required information from only CMU or CMX.

The angular distribution analysis is performed separately in each of the 12 ranges of dimuon mass shown in Fig. 1. The angular distributions of Υ decays are analyzed in eight ranges of $p_T(\Upsilon)$ from 0 to 40 GeV/c and are restricted to the central region of rapidity $|y(\Upsilon)| < 0.6$. For a given range of transverse momenta, the sample of dimuon candidates is divided into two subsamples according to whether one of the muons is reconstructed precisely using measurements from the silicon detector and its extrapolated trajectory misses the beam axis by a distance $|d_0| > 150$ μm. Events with at least one muon satisfying this requirement are referred to as the "displaced" sample since they are consistent with the presence of a long-lived

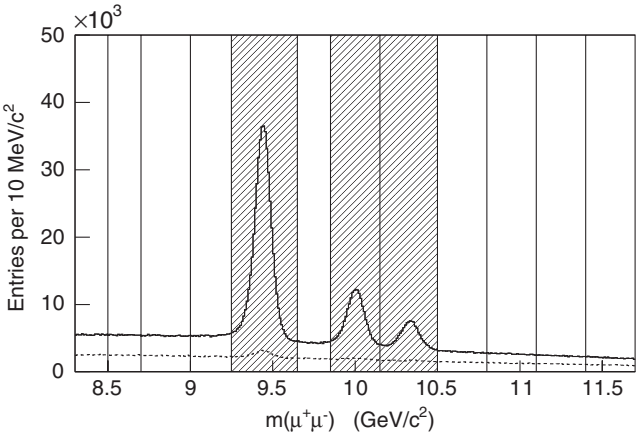

FIG. 1. Mass distribution of $\mu^+\mu^-$ candidates in the prompt (solid line) and displaced (dashed line) samples, with the ranges of invariant mass used to select the signal and sideband events indicated. Hatched regions indicate the three mass ranges containing the $\Upsilon(nS)$ signals.

parent particle, which is a characteristic feature of the dimuon background arising from semileptonic decays of heavy quarks. These criteria do not bias the angular distribution and, since the displaced sample contains almost no Υ signal, it provides a good description of the dimuon background that remains in the complementary ''prompt'' sample. We verify that this is the case by comparing the angular distributions of prompt and displaced samples projected onto the $\cos\theta$ and φ axes for mass ranges in the sidebands of the Υ signals. The level of agreement is quantified by computing the Kolmogorov-Smirnov statistic for each distribution, which suggests that any differences in their observed shapes are consistent with statistical fluctuations.

The prompt sample contains most of the $\Upsilon \to \mu^+\mu^-$ signal, while a small fraction is retained in the displaced sample due to the 30 μm resolution of the d_0 measurement (see Fig. 1). The fraction f_p that is present in the prompt sample is measured using a simultaneous binned likelihood fit to the dimuon mass distributions of both prompt and displaced samples. The Υ signals are described by Gaussian functions with common widths, their mass splittings constrained to the known values [16], and their yields scaled by f_p and $1 - f_p$ in the prompt and displaced samples, respectively. The value of f_p ranges from 96%–99% depending on the Υ p_T and whether the candidate was recorded with the central-central or central-forward trigger scenario.

A second fit is performed to measure the mass-dependent ratio $r(m)$ of the prompt and displaced mass distributions. This is similar to the first fit, but uses only the sidebands in the prompt sample, $m(\mu^+\mu^-) < 9$ GeV/c^2 or $m(\mu^+\mu^-) > 10.5$ GeV/c^2, to avoid the need to model the $\Upsilon(nS)$ line shapes. The mass distribution of the background in the displaced sample is parametrized by a gamma function at low p_T and by an exponential function at higher p_T. The mass distribution of background in the prompt sample is accurately described by the mass distribution in the displaced sample multiplied by a scale factor that varies linearly with mass, $r(m) = a + bm$, with the coefficients a and b determined from the fit. The value of the function $r(m_{\Upsilon(1S)})$, evaluated at the $\Upsilon(1S)$ mass, varies between 1.8–3.9 over the range of dimuon p_T considered. In the subsequent analysis of angular distributions, the value of this function and its uncertainty, both evaluated at the center of each mass range containing the Υ signals, are used to impose a Gaussian constraint on the background yield in the prompt sample.

The displaced sample provides a good description of the angular distribution of background in the prompt sample. This observation is consistent with all background arising from semileptonic decays of heavy quarks, or any small nonheavy flavor background component having the same angular distribution in prompt and displaced samples. We observe good agreement between the angular distributions in the prompt and displaced background, outside the Υ signal mass regions, even though the angular distributions change rapidly with dimuon mass and p_T. A typical example illustrating this comparison is shown in Fig. 2. We then proceed to use the displaced sample to constrain the angular distribution of the background when analyzing the angular distribution of muons from Υ decays.

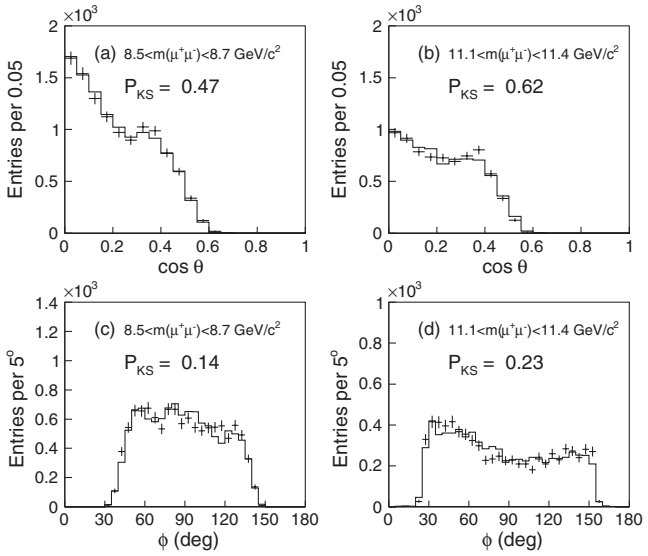

FIG. 2. Comparisons of projected angular distributions measured in the Collins-Soper frame for prompt (histograms) and displaced (error bars) dimuon samples in the low-mass (a), (c) and high-mass (b), (d) sidebands for events recorded with the central-central trigger. Displaced samples are normalized to the number of events in the corresponding prompt samples. The p value of the Kolmogorov-Smirnov statistic comparing each distribution is shown.

In mass ranges containing the Υ signals, we perform a third simultaneous fit, in both the prompt and displaced samples, to the distributions of angles $(\cos\theta, \varphi)$ collected in 20×36 discrete intervals. Separate fits are performed for the two cases in which the angles represent the direction of the positive muon with respect to the axes of the s-channel helicity frame or those of the Collins-Soper frame. For both frames, the angular distributions are described by linear combinations of probability density functions for signal and background components. We factor these functions into an underlying angular distribution, with that of the Υ signal parametrized using Eq. (1), and an acceptance function that accounts for the geometry of the muon detectors and the kinematic restrictions imposed by the trigger. The parameters in the underlying angular distributions for the Υ signal and for the background are determined using a simultaneous, binned likelihood fit in which the expected numbers of events in each discrete angular interval are expressed as

$$\frac{dN_p}{d\Omega_{ij}} \sim N_\Upsilon f_p \mathcal{A}_\Upsilon(\cos\theta_i, \varphi_j) w_\Upsilon(\cos\theta_i, \varphi_j; \vec{\lambda}_\Upsilon) + N_d s_p \mathcal{A}_b(\cos\theta_i, \varphi_j) w_b(\cos\theta_i, \varphi_j; \vec{\lambda}_b), \quad (2)$$

$$\frac{dN_d}{d\Omega_{ij}} \sim N_\Upsilon(1-f_p)\mathcal{A}_\Upsilon(\cos\theta_i,\varphi_j)w_\Upsilon(\cos\theta_i,\varphi_j;\vec{\lambda}_\Upsilon) + N_d\mathcal{A}_b(\cos\theta_i,\varphi_j)w_b(\cos\theta_i,\varphi_j;\vec{\lambda}_b). \quad (3)$$

In these expressions, N_Υ and N_d are the Υ and displaced background event yields, f_p is the fraction of the Υ signal in the prompt sample, and s_p is the ratio of the background yields in the prompt and displaced samples, which is Gaussian-constrained to $r(m)$. The acceptance for signal $\mathcal{A}_\Upsilon$ and background $\mathcal{A}_b$, which are calculated separately, are described below. The modeling of the background angular distribution is improved by imposing the additional kinematic restriction $|p_T(\mu^+) - p_T(\mu^-)| < (p_T(\mu^+\mu^-) - 0.5\ \mathrm{GeV}/c)$, which removes back-to-back muons that have large values of $\cos\theta$ in the s-channel helicity frame. This has a negligible effect on the $\Upsilon(nS)$ acceptance for $p_T(\Upsilon) > 6\ \mathrm{GeV}/c$. The angular distributions for Υ signal w_Υ and background w_b are described by sets of parameters $\vec{\lambda}_\Upsilon$ and $\vec{\lambda}_b$. For the signal, w_Υ has the form of Eq. (1), whereas $w_b(\cos\theta, \varphi; \vec{\lambda}_b)$ has, in addition to the terms in Eq. (1), an empirical $\lambda_4\cos^4\theta$ term that parametrizes the background shape more accurately in some ranges of p_T and invariant mass. The free parameters in the fit are N_Υ, N_d, s_p, $\vec{\lambda}_\Upsilon$, and $\vec{\lambda}_b$, while f_p is fixed to the value determined previously from the first fit to the dimuon mass distributions.

The detector acceptance is calculated using a Monte Carlo (MC) simulation in which dimuon events generated with isotropic distributions of decay angles are processed using the standard CDF II detector simulation and event reconstruction programs. Separate samples are simulated at fixed masses to calculate the acceptance for the three $\Upsilon(nS)$ signals, while the acceptance for the dimuon background is calculated using a continuum of dimuon invariant masses ranging from 8 to 12 GeV/c^2.

Figure 3 shows distributions for the data and the best fit model in one of the ranges of dimuon p_T in the mass range containing the $\Upsilon(1S)$ signal. The shapes of the projected distributions are primarily determined by the acceptance, since the resolution with which $\cos\theta$ and φ are measured is much smaller than the binning chosen for the fit. However, the agreement between the data and the model in regions where the acceptance changes rapidly demonstrates that resolution effects are modeled accurately in the detector simulation. No significant discrepancy between the data and the fit model is observed in χ^2 tests applied to one-dimensional projected distributions over the analyzed range of the dimuon mass and p_T.

Systematic uncertainties on the parameters λ_θ, λ_φ, and $\lambda_{\theta\varphi}$ due to the limited precision with which the trigger and reconstruction efficiencies are determined are evaluated by repeating the analysis with acceptances recalculated with all efficiencies simultaneously varied by $\pm 1\sigma$. The resulting change in the fitted parameters provides a conservative estimate of the sensitivity to the measured acceptance. Because the measured parameters depend on the estimated background in the prompt sample, an alternate, quadratic parametrization of the function $r(m)$ was also investigated. The resulting small variations in the fitted angular

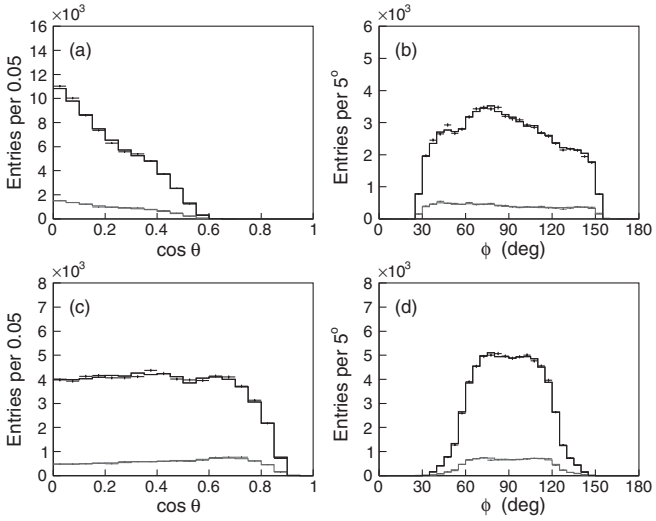

FIG. 3. Examples of projections of angular variables measured in the Collins-Soper (a), (b) and the s-channel helicity (c), (d) frames for the range of invariant mass containing the $\Upsilon(1S)$ signal with $4 < p_T < 6\ \mathrm{GeV}/c$ and recorded with the central-central trigger. The prompt sample is shown in black while the displaced sample is shown in grey. The distributions from collision data are shown with error bars and the results of the fits are indicated by the histograms.

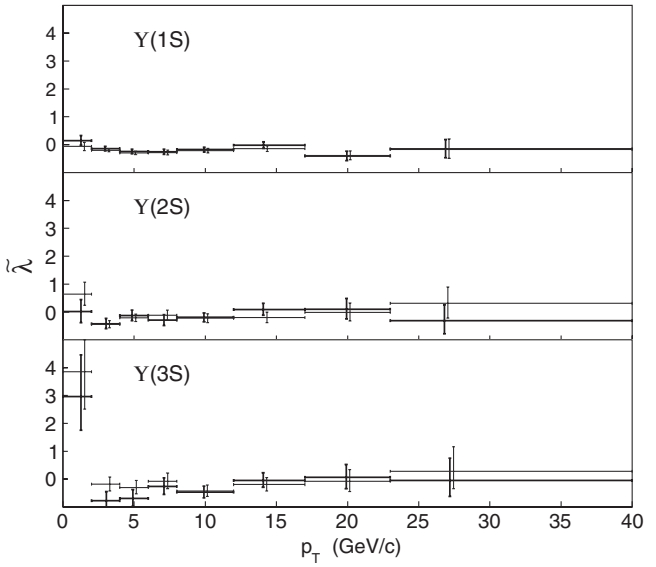

FIG. 4. Rotational invariant $\tilde{\lambda}$ as a function of $p_T(\Upsilon)$ for the $\Upsilon(1S)$, $\Upsilon(2S)$, and $\Upsilon(3S)$ states. Values of $\tilde{\lambda}$ calculated in the Collins-Soper frame are indicated by dark lines, while those calculated in the s-channel helicity frame are indicated by grey lines and are horizontally offset to slightly larger p_T values for clarity.

TABLE I. Values of λ_θ, measured in the s-channel helicity frame for each range of $p_T(\Upsilon)$. The first uncertainty is statistical while the second uncertainty is systematic and is described in the text.

p_T(GeV/c)	$\lambda_\theta[\Upsilon(1S)]$	$\lambda_\theta[\Upsilon(2S)]$	$\lambda_\theta[\Upsilon(3S)]$
0–2	$0.01 \pm 0.10 \pm 0.05$	$-0.07 \pm 0.20 \pm 0.05$	$0.32 \pm 0.36 \pm 0.12$
2–4	$-0.08 \pm 0.04 \pm 0.03$	$-0.29 \pm 0.10 \pm 0.06$	$-0.19 \pm 0.17 \pm 0.08$
4–6	$-0.11 \pm 0.04 \pm 0.03$	$-0.11 \pm 0.10 \pm 0.05$	$-0.01 \pm 0.19 \pm 0.09$
6–8	$-0.12 \pm 0.06 \pm 0.04$	$-0.09 \pm 0.12 \pm 0.07$	$-0.48 \pm 0.14 \pm 0.13$
8–12	$-0.15 \pm 0.06 \pm 0.02$	$-0.18 \pm 0.11 \pm 0.03$	$0.07 \pm 0.18 \pm 0.04$
12–17	$-0.13 \pm 0.08 \pm 0.04$	$-0.09 \pm 0.15 \pm 0.08$	$0.14 \pm 0.22 \pm 0.07$
17–23	$-0.23 \pm 0.13 \pm 0.08$	$0.06 \pm 0.25 \pm 0.12$	$0.14^{+0.36}_{-0.33} \pm 0.12$
23–40	$-0.21 \pm 0.24 \pm 0.11$	$0.00^{+0.39}_{-0.33} \pm 0.16$	$0.14^{+0.50}_{-0.42} \pm 0.13$

distribution parameters are treated as an additional systematic uncertainty. Finally, the contribution of the uncertainty in the fitted parameters due to the finite MC sample size used to calculate the acceptance was estimated using ensembles of MC simulations with the same size used in the analysis of the data. The uncertainties due to finite MC sample size and the determination of efficiencies are at most 30% of the size of the statistical uncertainty for the three $\Upsilon(nS)$ states, while the uncertainty due to the treatment of the prompt scale factor function is no more than 20% of the statistical uncertainty.

Figure 4 shows the rotational invariant $\tilde{\lambda}$ which is calculated from the measured values of λ_θ and λ_φ in each p_T range for both the Collins-Soper and s-channel helicity frames. Uncertainties in $\tilde{\lambda}$ measured in the two coordinate frames are highly correlated. Monte Carlo simulations are used to calculate the expected sizes of differences between the two values of $\tilde{\lambda}$ and in most cases, the observed deviations are found to be consistent with purely statistical fluctuations. A systematic uncertainty derived from the difference between $\tilde{\lambda}$ measured in the two coordinate frames is only significant for the lowest three p_T ranges of the $\Upsilon(3S)$. In the lowest p_T range, the values of $\tilde{\lambda}$ measured for the $\Upsilon(3S)$ differ by 2.4σ, without accounting for systematic uncertainties, and this is the only case where the angular distribution is observed to be significantly nonisotropic. However, we cannot find any evidence to suggest that this is due to a bias or systematic effect since we do not see a similar trend for the $1S$ and $2S$ states and can find no anomalous behavior in any of the underlying distributions.

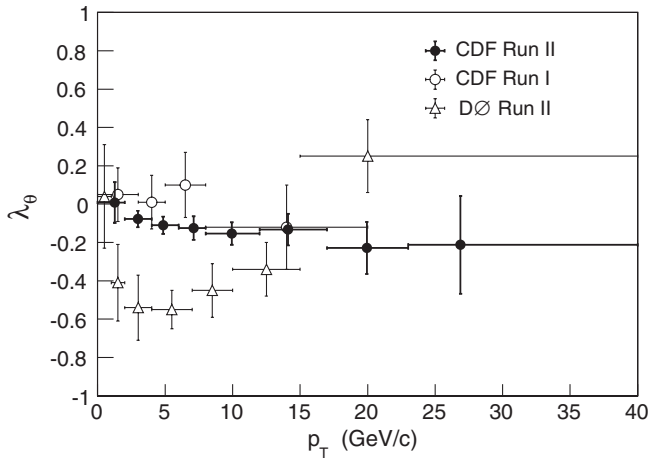

FIG. 5. Comparison of the λ_θ parameter measured for $\Upsilon(1S)$ decays in the s-channel helicity frame (solid symbols) with previous measurements from the CDF [4] (open circles) and the D0 [18] (open triangles) experiments.

The values of $\tilde{\lambda} \approx 0$ suggest that the decays of all three $\Upsilon(nS)$ resonances are consistent with an unpolarized mixture of states. Table I lists the values of λ_θ measured in the s-channel helicity frame for the $\Upsilon(1S)$, $\Upsilon(2S)$, and $\Upsilon(3S)$ states, with the systematic uncertainties described above added in quadrature [17]. Figure 5 shows a comparison of the λ_θ parameter, measured for the $\Upsilon(1S)$ state in the s-channel helicity frame, with previous measurements. The current result is found to be statistically consistent with the previous measurement from CDF [4], which was made for $|y| < 0.4$ at $\sqrt{s} = 1.8$ TeV rather than $|y| < 0.6$ and $\sqrt{s} = 1.96$ TeV. Restricting the current measurement to $|y| < 0.4$ does not change the results appreciably. The current $\Upsilon(1S)$ result is inconsistent with the previous measurement from the D0 experiment [18] at the level of 4.5σ.

In conclusion, we have measured the angular distributions of muons from $\Upsilon(1S)$, $\Upsilon(2S)$, and $\Upsilon(3S)$ decays with $|y| < 0.6$ and in several ranges of transverse momentum up to 40 GeV/c. We find that the decay-angle distributions of all three $\Upsilon(nS)$ states are nearly isotropic, as was suggested by previous measurements [4] in the case of the $\Upsilon(1S)$. This is the first measurement to simultaneously determine the three parameters needed to fully quantify the angular distribution of $\Upsilon(nS) \to \mu^+\mu^-$ decays. This is also the first analysis to present information on the angular distribution of $\Upsilon(3S)$ mesons produced in high energy $p\bar{p}$ collisions.

We thank the Fermilab staff and the technical staffs of the participating institutions for their vital contributions. This work was supported by the U.S. Department of Energy and National Science Foundation; the Italian

Istituto Nazionale di Fisica Nucleare; the Ministry of Education, Culture, Sports, Science and Technology of Japan; the Natural Sciences and Engineering Research Council of Canada; the National Science Council of the Republic of China; the Swiss National Science Foundation; the A. P. Sloan Foundation; the Bundesministerium für Bildung und Forschung, Germany; the Korean World Class University Program, the National Research Foundation of Korea; the Science and Technology Facilities Council and the Royal Society, UK; the Russian Foundation for Basic Research; the Ministerio de Ciencia e Innovación, and Programa Consolider-Ingenio 2010, Spain; the Slovak R&D Agency; the Academy of Finland; and the Australian Research Council (ARC).

[a]Deceased.
[b]Visitor from Istituto Nazionale di Fisica Nucleare, Sezione di Cagliari, 09042 Monserrato (Cagliari), Italy.
[c]Visitor from University of CA Irvine, Irvine, CA 92697, USA.
[d]Visitor from University of CA Santa Barbara, Santa Barbara, CA 93106, USA.
[e]Visitor from University of CA Santa Cruz, Santa Cruz, CA 95064, USA.
[f]Visitor from Institute of Physics, Academy of Sciences of the Czech Republic, Czech Republic.
[g]Visitor from CERN, CH-1211 Geneva, Switzerland.
[h]Visitor from Cornell University, Ithaca, NY 14853, USA.
[i]Visitor from University of Cyprus, Nicosia CY-1678, Cyprus.
[j]Visitor from Office of Science, U.S. Department of Energy, Washington, DC 20585, USA.
[k]Visitor from University College Dublin, Dublin 4, Ireland.
[l]Visitor from ETH, 8092 Zurich, Switzerland.
[m]Visitor from University of Fukui, Fukui City, Fukui Prefecture, Japan 910-0017.
[n]Visitor from Universidad Iberoamericana, Mexico D.F., Mexico.
[o]Visitor from University of Iowa, Iowa City, IA 52242, USA.
[p]Visitor from Kinki University, Higashi-Osaka City, Japan 577-8502.
[q]Visitor from KS State University, Manhattan, KS 66506, USA.
[r]Visitor from Korea University, Seoul, 136-713, Korea.
[s]Visitor from University of Manchester, Manchester M13 9PL, United Kingdom.
[t]Visitor from Queen Mary, University of London, London, E1 4NS, United Kingdom.
[u]Visitor from University of Melbourne, Victoria 3010, Australia.
[v]Visitor from Muons, Inc., Batavia, IL 60510, USA.
[w]Visitor from Nagasaki Institute of Applied Science, Nagasaki, Japan.
[x]Visitor from National Research Nuclear University, Moscow, Russia.
[y]Visitor from Northwestern University, Evanston, IL 60208, USA.
[z]Visitor from University of Notre Dame, Notre Dame, IN 46556, USA.
[aa]Visitor from Universidad de Oviedo, E-33007 Oviedo, Spain.
[bb]CNRS-IN2P3, Paris, F-75205 France.
[cc]Texas Tech University, Lubbock, TX 79609, USA.
[dd]Universidad Tecnica Federico Santa Maria, 110v Valparaiso, Chile.
[ee]Yarmouk University, Irbid 211-63, Jordan.

[1] F. Abe *et al.* (CDF Collaboration), Phys. Rev. Lett. **79**, 572 (1997); **75**, 4358 (1995).
[2] E. Braaten, M. A. Doncheski, S. Fleming, and M. L. Mangano, Phys. Lett. B **333**, 548 (1994); M. Cacciari and M. Greco, Phys. Rev. Lett. **73**, 1586 (1994).
[3] T. Affolder *et al.* (CDF Collaboration), Phys. Rev. Lett. **85**, 2886 (2000).
[4] D. Acosta *et al.* (CDF Collaboration), Phys. Rev. Lett. **88**, 161802 (2002).
[5] P. Cho and A. K. Leibovich, Phys. Rev. D **53**, 150 (1996); **53**, 6203 (1996).
[6] P. Faccioli, C. Lourenço, J. Seixas, and H. K. Wohri, Phys. Rev. Lett. **102**, 151802 (2009); Eur. Phys. J. C **69**, 657 (2010); P. Faccioli, C. Lourenço, and J. Seixas, Phys. Rev. Lett. **105**, 061601 (2010); Phys. Rev. D **81**, 111502(R) (2010).
[7] J. C. Collins and D. E. Soper, Phys. Rev. D **16**, 2219 (1977).
[8] M. Noman and S. D. Rindani, Phys. Rev. D **19**, 207 (1979).
[9] Rotational invariance of $\tilde{\lambda}$ follows from the invariance of the expression $\sum_{n=-J}^{J}(-1)^n\langle\psi|n\rangle\langle -n|\psi\rangle$, in which $|\psi\rangle$ is a general state vector for a particle of spin J and $|n\rangle$ are the standard J_z basis eigenstates.
[10] A. Sill *et al.*, Nucl. Instrum. Methods Phys. Res., Sect. A **447**, 1 (2000); C. S. Hill, *ibid.* **530**, 1 (2004).
[11] T. Affolder *et al.*, Nucl. Instrum. Methods Phys. Res., Sect. A **526**, 249 (2004).
[12] G. Ascoli, L. E. Holloway, I. Karliner, U. E. Kruse, R. D. Sard, V. J. Simaitis, D. A. Smith, and T. K. Westhusing, Nucl. Instrum. Methods Phys. Res., Sect. A **268**, 33 (1988).
[13] A. Artikov *et al.*, Nucl. Instrum. Methods Phys. Res., Sect. A **538**, 358 (2005).
[14] E. J. Thomson *et al.*, IEEE Trans. Nucl. Sci. **49**, 1063 (2002).
[15] T. Aaltonen *et al.* (CDF Collaboration), Phys. Rev. Lett. **107**, 239903 (2011); **100**, 101802 (2008); D. Acosta *et al.* (CDF Collaboration), *ibid.* **93**, 032001 (2004).
[16] K. Nakamura *et al.* (Particle Data Group), J. Phys. G **37**, 075021 (2010).
[17] See Supplemental Material at http://link.aps.org/supplemental/10.1103/PhysRevLett.108.151802 for complete tables of results for λ_θ, λ_φ, $\lambda_{\theta\varphi}$, and $\tilde{\lambda}$ in both the s-channel helicity frame and Collins-Soper frame for the $\Upsilon(1S)$, $\Upsilon(2S)$, and $\Upsilon(3S)$.
[18] V. M. Abazov *et al.* (D0 Collaboration), Phys. Rev. Lett. **101**, 182004 (2008).